

Modulator structures for radio-on-fiber applications

Sean V. Hum, Michał Okoniewski, and Robert J. Davies

Abstract — Traditional electro-optic modulators are not optimized for bandpass applications such as radio-on-fiber delivery systems due to their limited electro-optic response. This paper presents a resonant electrode structure that can be employed in optical modulator designs to enhance the electro-optic response of the modulator over a narrow frequency band, and improve the performance of optical radio systems. A simple model of the structure is developed, and experimental results validating the model and illustrating the effectiveness of the structure are presented.

Keywords — resonators, electro-optic modulators, microwave photonics, radio-on-fiber, optical modulation.

1. Introduction

Radio-on-fiber is an emerging and attractive architecture for optical distribution of radio signals in wireless delivery systems [1–3]. In traditional wireless delivery systems based on optical distribution networks, baseband signals are transported to base stations where they are upconverted to the operating radio frequency and transmitted to subscribers. In radio-on-fiber delivery systems, the actual radio signals are transported over the optical fiber network to the base stations on optical subcarriers, eliminating the need for costly RF conversion equipment at the remote sites and lowering overall system costs. A diagram of the downlink in a general radio-on-fiber system is shown in Fig. 1. Such systems have been proposed extensively for use in mobile communications systems and have most recently found applications in high capacity millimetre-wave transmission systems [4].

The electro-optic modulator at the transmitter, typically a Mach-Zehnder modulator (MZM), plays a crucial role in determining the performance of radio-on-fiber systems. The RF link gain between the input to the optical modulator and the output of the optical detector is largely determined by the depth of modulation that can be developed at the transmitter, which in turn depends on the V_π or switching voltage of the modulator. In fact, it can be easily shown that the link gain of the downlink is given by [5]

$$G = \frac{\mathcal{R}^2 G_o^2 P_{oin}^2 \pi^2 R_{MZM} R_{det}}{V_\pi^2}, \quad (1)$$

where \mathcal{R} is the responsivity of the photodetector in A/W, G_o is the gain of the optical link, P_{oin} is the optical source power, R_{MZM} is the termination resistance of the MZM elec-

trode, and R_{det} is the termination resistance of the detector. Unfortunately, the RF link loss tends to be very large, on the order of 30 dB or greater, even if there is negligible optical loss in the fiber and the responsivity of the optical detector is very high (nearing the quantum limit). Therefore, efforts have focused on reducing the V_π of electro-optic modulators in order to address this problem.

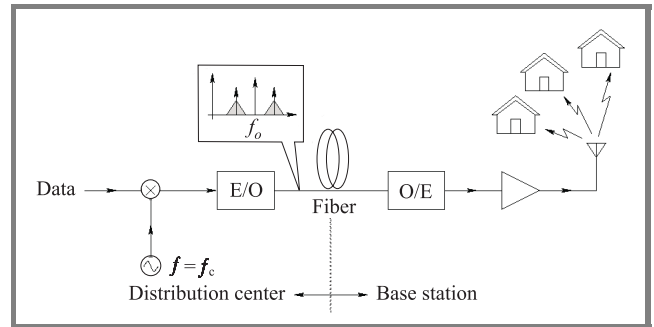


Fig. 1. The downlink of a general radio-on-fiber delivery system: E/O – electrical-to-optical conversion, O/E – optical-to-electrical conversion.

Traditional MZM designs have relatively high V_π values, due to the travelling-wave electrode structure used in each of the phase modulation arms of the MZM. One of these electrodes is shown schematically in Fig. 2a. The transmission line forming the electrode has a propagation constant $\gamma = \alpha + j\beta$ and characteristic impedance Z_0 , and is terminated in matched load. This structure provides optical modulators with very high bandwidth capabilities to make them compatible with broadband digital systems such as OC-192, but develops relatively weak fields across the active region of the modulator, leading to a weak electro-optic effect and high V_π . Since broadband modulator performance is not a prerequisite for radio-on-fiber systems, it raises the possibility of optimizing the modulator for bandpass operation.

Resonant modulator electrode structures, first proposed for picosecond optical samplers [6], have emerged as a promising technique for reducing the switching voltage of electro-optic modulators. In these structures, the modulating electrode is transformed into a resonant cavity across which high electric field strength can be developed at the resonant frequency of the structure, lowering the V_π of the device. Hence, the bandwidth of the travelling-wave structure is sacrificed in order to yield a stronger electro-optic response. Resonant modulators have found application in op-

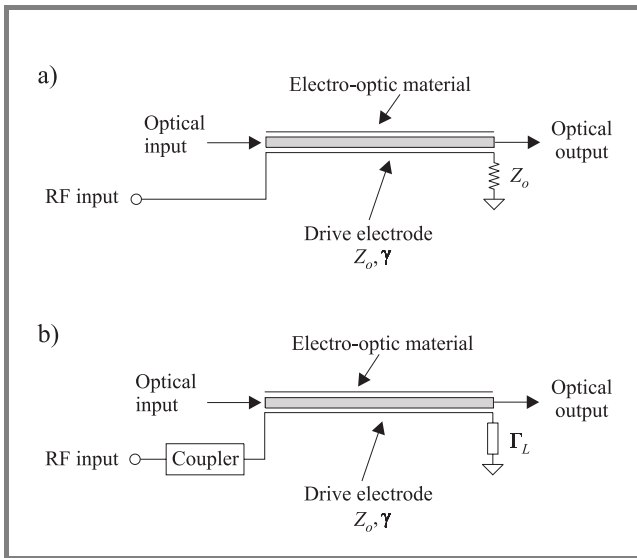


Fig. 2. Electrode structures for optical phase modulators in a MZM: (a) travelling-wave electrode structure; (b) resonant electrode structure.

tical phase modulators [7, 8], and have more recently been studied for use in analog and radio-on-fiber links [9–11]. This paper presents the design of several resonant electrode structures for optical modulators. A simple model for the structures is derived, and the model validated against experimental results. Experimental results also demonstrate the potential of resonant modulator designs in radio-on-fiber systems.

2. The resonant electrode structure

In a resonant electrode structure, shown in generalized form in Fig. 2b, the travelling-wave termination shown in Fig. 2a is removed and replaced with an electrical reflector with reflection coefficient Γ_L . A coupler is introduced at the input to the electrode, transforming the modulation arm into a resonant cavity whereby multiple reflections between the reflector and the coupler combine to produce a standing wave of increased amplitude relative to that achievable with the corresponding travelling-wave structure. This improves the electro-optic effect around the resonant frequency of the structure, lowering the V_π of the device. The phase imparted to the optical wave depends on the field profile $E(z)$ seen by an optical wave as it travels through the modulator arm. If $\Delta\phi(t_0)$ denotes the phase imparted to an optical wave incident to the modulator arm at time t_0 , the expression for $\Delta\phi(t_0)$ is given by [6]

$$\Delta\phi(t_0) = \int_{t_0}^{t_0+L/v_o} \frac{\pi r n^3 E[z = v_o(t-t_0), t] v_o dt}{\lambda_0}, \quad (2)$$

where L denotes the active region length, v_o is the optical phase velocity, n is the effective refractive index of the optical waveguide, r is Pockel's coefficient for the electro-optic material used, and λ_0 is the free space wavelength

of the optical carrier. The field profile seen by the optical wave as a function of the position z along the modulator arm can be represented using a signal flow graph (SFG) with the electrode partitioned into two sections of length z and length $L-z$ and determining the amplitudes of the forward- and reverse-travelling waves within the cavity. The envelope $U(z)$ of the standing wave relative to the incident wave is then readily found as

$$U(z) = U_0 (e^{-\gamma z} + \Gamma_L e^{-2\gamma L + \gamma z}), \quad (3)$$

where

$$U_0 = \frac{s_{21}}{1 - s_{22} e^{-2\gamma L} \Gamma_L} \quad (4)$$

and s_{ij} are the scattering parameters of the coupler. Generally, the reflector and coupler are chosen so that envelope of the field profile developed across the active region is symmetric with respect to the centre of the active region so that the expression (2) is maximized. For example, a mode which develops a field profile $|E(z)| \propto \sin(\beta z)$, $0 \leq \beta z \leq \pi$, is often employed. For simplicity, this mode will be considered in the analysis of the cavity. It is readily achieved using a short-circuited modulator electrode ($\Gamma_L = -1$) and a shunt-inductive coupler, as shown schematically in Fig. 3.

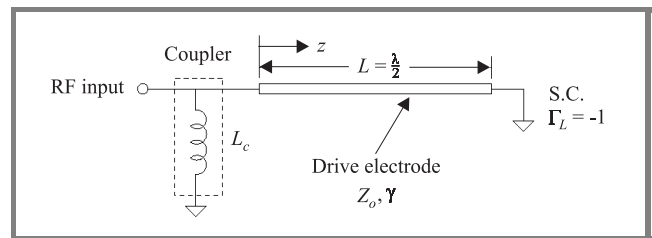


Fig. 3. Inductively-coupled half-wavelength resonator.

At resonance, the transmission coefficient of the coupling inductance is given by

$$|s_{21}| = \frac{2\omega_c L_c}{\sqrt{Z_0^2 + 4\omega_c^2 L_c^2}}, \quad (5)$$

where L_c denotes the coupling inductance and ω_c is the radian resonant frequency. For critical coupling into the cavity, which maximizes power transfer to the cavity and the corresponding electric field developed across the active region, the required coupling inductance can be found using a similar technique presented in [12] and is given by

$$L_c = \frac{Z_0}{\omega_c} \sqrt{\frac{\pi}{2Q_u}} \quad (6)$$

for a short-circuited $\lambda/2$ resonator. Q_u denotes the unloaded quality factor of the resonator. Substituting the

expression for the optimum coupling inductance given by Eq. (6) into Eq. (5) and simplifying yields

$$|s_{21}| = \sqrt{\frac{2\pi}{Q_u + 2\pi}}. \quad (7)$$

Next, consider the denominator of Eq. (4). At resonance, the denominator of this equation becomes an entirely real quantity because of the necessary condition for resonance that the loop gain $s_{22}e^{-2\gamma L}\Gamma_L$ be a real quantity. At resonance the loop gain is equal to $e^{-2\alpha_{eff}L}$, where α_{eff} is the apparent distributed attenuation factor of the cavity which accounts for any power lost from the reflector (if $|\Gamma_L| \neq 1$) and leakage back through the coupler. It is defined as

$$\alpha_{eff} = \alpha + \frac{1}{2L} \ln \left(\frac{1}{|\Gamma_L||s_{22}(\omega_c)|} \right). \quad (8)$$

Since the unloaded Q of the cavity Q_u is twice the loaded Q of the cavity $Q_l = \beta/2\alpha_{eff}$, and $2\beta L \approx 2\pi$ at resonance,

$$e^{-2\alpha_{eff}L} = e^{-2\beta L/Q_u} \approx e^{-2\pi/Q_u} \quad (9)$$

and the equation for U_0 can be written as

$$U_0 = \frac{\sqrt{2\pi/(Q_u + 2\pi)}}{1 - e^{-2\pi/Q_u}}. \quad (10)$$

The maximum field developed in the cavity is then given by

$$E_{max} = E_0 U_0 |e^{-\gamma z} + \Gamma_L e^{-2\gamma L + \gamma z}|, \quad (11)$$

where E_0 is the amplitude of the incident electric field. If $\alpha L \ll 1$, which is the case for any practical resonator, then the maximum value of $|e^{-\gamma z} + \Gamma_L e^{-2\gamma L + \gamma z}|$ is approximately 2. Hence, the peak field enhancement factor of the resonator is given by

$$F = \frac{E_{max}}{E_0} = \frac{2\sqrt{2\pi/(Q_u + 2\pi)}}{1 - e^{-2\pi/Q_u}}. \quad (12)$$

This equation relates the field enhancement factor offered by the resonator as a function of unloaded resonator Q. While it was derived for an inductively-coupled half-wave resonator, it can be shown this expression remains unchanged for other types of resonator configurations (for example, capacitively-coupled resonators or resonators employing higher order modes), provided that the critical coupling condition into the cavity is maintained.

If the shape of the standing-wave field envelope developed across the active region is known, then Eqs. (12) and (2) can be used to predict the overall phase imparted to the optical wave. For example, for the simple resonator case used in the development, $E(z) \approx FE_0 \sin(\beta z)$. However, in general passive sections of feedline may also form part of the resonant cavity, which causes a fraction of this field profile to be developed across the active region of the modulator. If the coupler and reflector are chosen to symmetrize the

field profile developed across the active region, this feedline acts to flatten the electric field profile which improves the modulation response further at the expense of lowering the resonant frequency of the structure. While this feedline may be purposefully added to achieve this effect, generally it is desirable to minimize the cavity loss as much as possible. The analysis will consider the case of arbitrary feedline length.

To determine the optical modulation enhancement factor P over a travelling-wave modulator, the integration of Eq. (2) is carried out for a modulator arm with total electrode length L_t and active region length $L < L_t$, with the active region centred across the electrode. The resulting expression for P is

$$\begin{aligned} P &= \frac{\Delta\phi}{\Delta\phi_{TW}} \\ &= \frac{v_o F}{L} \left\{ \frac{L_t}{\omega L_t - \pi v_o} \sin \left(\frac{\omega L}{2v_o} - \frac{\pi L}{2L_t} \right) + \right. \\ &\quad \left. + \frac{L_t}{\omega L_t + \pi v_o} \sin \left(\frac{\omega L}{2v_o} + \frac{\pi L}{2L_t} \right) \right\}, \quad (13) \end{aligned}$$

where $\Delta\phi_{TW}$ is the phase induced by a corresponding travelling-wave modulator with the same geometry. For more complicated resonator configurations, the exact modulation improvement can be determined by computing the exact standing-wave envelope using signal flow graph analysis of the structure, and using Eq. (2) to determine the phase imparted to the optical wave.

Converting a standard travelling-wave electrode design to a resonantly-enhanced electrode is an effective method for reducing the apparent V_π of the device over a narrow frequency range. It is important to realize that resonantly-enhanced modulators are not meant to replace other techniques for reducing the V_π of electro-optic modulators, but rather merged with these techniques to further lower V_π figures. The true value of a resonant-enhancement techniques lies in the fact that it can be integrated with almost any arbitrary electrode geometry, provided that the reduction in bandwidth is acceptable. Hence, recent advances in low- V_π travelling-wave modulators can be used in conjunction with a resonant electrode to achieve ultra-low V_π values.

3. Designs and results

Practically, resonantly-enhanced electrode structures can be realized in two ways. First, the coupler and reflector can be patterned directly with the modulator electrode to create a fully integrated resonant modulator electrode. The second approach is to use a packaged electro-optic modulator and attach the coupler and reflector externally, yielding a so-called externally-resonated design. Ultimately, the former method yields the best results since integrated designs achieve inherently L_t/L ratios close to unity, yielding devices with the highest resonant frequency and the lowest cavity losses. However, to validate the concepts presented

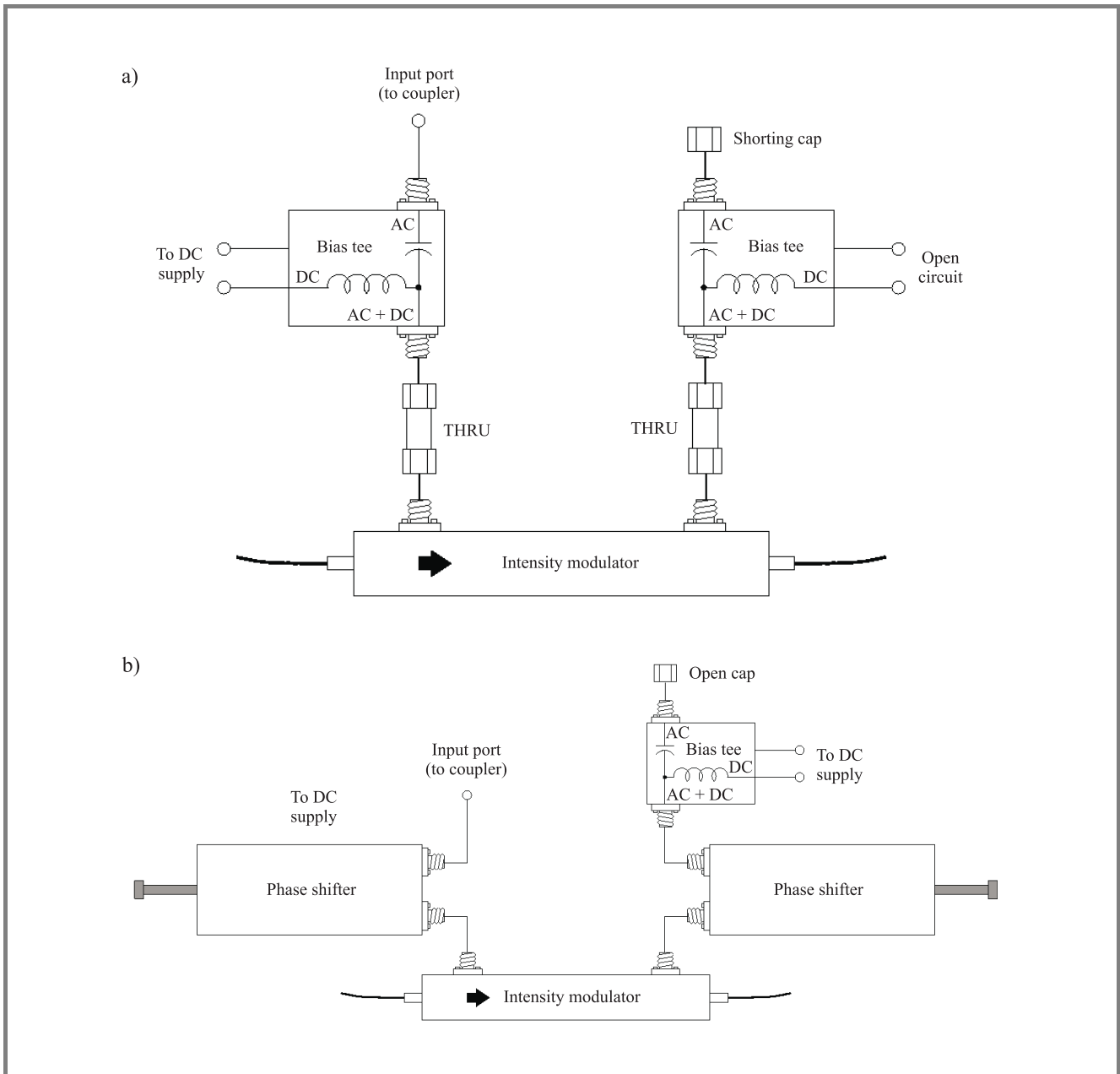


Fig. 4. Externally-resonated modulator designs: (a) basic design (I); (b) design with adjustable field confinement (III-IV).

in this paper, the latter approach was taken for ease of experimentation.

Several externally-resonated modulator structures were constructed using several off-the-shelf MZM's. Four designs were evaluated in all. The first design, shown in Fig. 4a, achieved minimal confinement of the half-wave field profile to the active region (i.e. a large L_t/L ratio) due to the large delay of the bias tees which increased the overall electrical cavity length. The second design (not shown) mitigated this problem to some extent through the use of an external DC bias electrode. Successive designs used higher-order resonant modes with the structure shown in Fig. 4 to achieve active region field profiles closer to the desired half-wavelength standing-wave shape. Phase shifters allowed

both the resonant frequency of the device to be changed as well as the spatial position of the standing wave to be moved within the cavity. The ultimate goal of these designs was to emulate a fully-integrated resonant modulator with $L_t/L = 1$.

Resonator couplers were realized using CPW shunt stub circuits (for the inductively-coupled designs) and CPW series stub circuits (for the capacitively-coupled, higher-order mode resonator designs). All the couplers were designed to provide critical coupling into the cavity and to minimize the additional electrical length added to the cavity.

The resonant modulator designs were embedded in an experimental prototype of a radio-on-fiber delivery system and the RF link gain of the system characterized using

a standard network analyzer. Experimental results showing the link loss reduction and bandwidths achieved with the prototypes are summarized in Table 1. Theoretical reductions in link loss are shown in parentheses. Note that for the resonator configurations employing higher-order modes, the effective L_t/L ratio was computed using the known active region length L and $L_t = \lambda/2$ for the effective cavity length.

Table 1
Calculated and measured resonant modulator parameters

Parameter	I	II	III	IV
f_r [MHz]	462.5	780.0	1195.5	1499.2
L/L_t [%]	33	58	72	100
Link loss reduction [dB]	9.1 (8.6)	6.8 (7.1)	4.0 (4.4)	2.7 (2.1)
V_π reduction [%]	65	54	37	26
3 dB trans. bandwidth [%]	13.7	16.5	5.0 (30.1)	4.9 (38.8)
10 dB R.L. bandwidth [%]	4.2	5.5	1.7 (10.2)	1.6 (12.8)

All the modulators provided substantial gain over their travelling-wave counterparts, with link gain enhancement ranging from 2.7 dB for the highest frequency resonator to over 9 dB for the lowest frequency resonator. As expected, the link gain enhancement was reduced as the resonant frequency of the structures increased due to increasing cavity loss, and greater confinement of the half-wave profile to the active region (which reduces the L_t/L ratio, corresponding P/F ratio, and the modulation improvement). Nevertheless, significant reductions in V_π were achieved (26–65% depending on the resonator configuration), illustrating the effectiveness of the resonant enhancement technique.

The bandwidth offered by the resonator structures was excellent, around 15% for the first two designs. Designs employing higher-order mode resonators had correspondingly reduced bandwidths due to the narrowband nature of the resonators, but the bandwidth of an integrated modulator that achieves the same level of field confinement could be expected to be much greater (corresponding to the bandwidths in square parentheses in Table 1). The highest frequency tested was 1500 MHz, where the $n = 8$ resonant mode was employed to develop exactly half a wavelength across the active region across one of the arms in the packaged MZM.

The table also illustrates that the simple model used to predict the field enhancement of the structures was very accurate, with the maximum error in the predicted modulation enhancement less than 8%. Hence, the developed expressions can be used to approximate the performance of externally-resonated designs and should be equally applicable to integrated designs.

Graphs of the measured link gain improvement for all four designs are shown Fig. 5, plotted along a frequency-

normalized abscissa. The curves for the higher-order resonant mode designs were also frequency scaled to illustrate potential operation for these devices if resonance had been achieved using the fundamental mode (corresponding to the situation in an integrated device) instead of a higher-order mode. The return loss for each of the structures is also plotted. The tradeoffs between the designs is immediately apparent, with low frequency designs offering the greatest gain due to lower cavity loss at those frequencies and maximum P/F values due to fairly large L_t/L ratios.

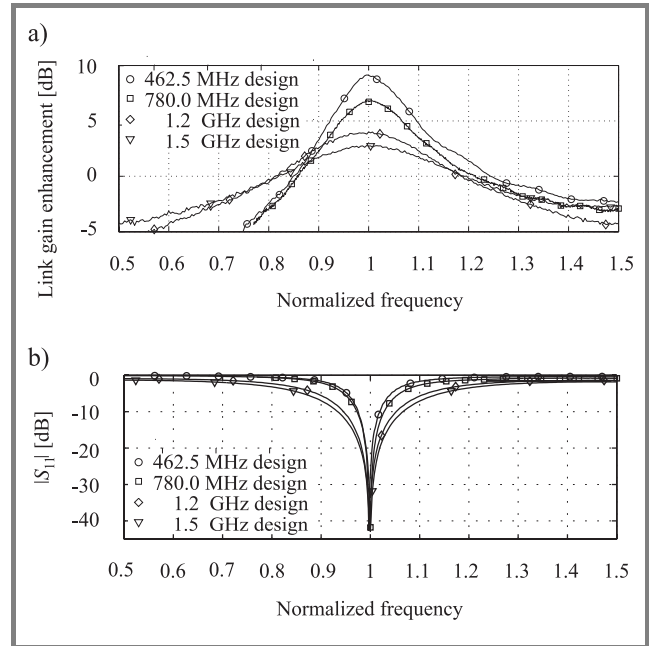


Fig. 5. Frequency-normalized link gain (a) and return loss (b).

As discussed earlier, signal flow graphs are useful for computing the exact field profile developed across the active region. This profile can then be used to accurately determine the improvement in modulation depth offered by an arbitrary resonator configuration. SFGs are also useful for characterizing the gain of a resonantly-enhanced modulator as a function of frequency. This study included an assessment of the accuracy of the SFG model used to derive expression (12). SFGs are well suited to analyzing the externally-resonated structures because the scattering parameters of the external components can be readily measured and integrated into the signal flow graph. Furthermore, it is anticipated that the SFG approach will be highly useful in developing more sophisticated resonator circuits, as well as analyzing integrated resonant modulator designs where more complicated circuit models of the electrode may be required.

Figure 6 illustrates the modulation improvement and input reflection coefficient predicted using the SFG model of two of the externally-resonated modulator structures. There is a clear correlation between measured and predicted results, and performing an SFG analysis of the structures actually resolved the small differences between the predictions of

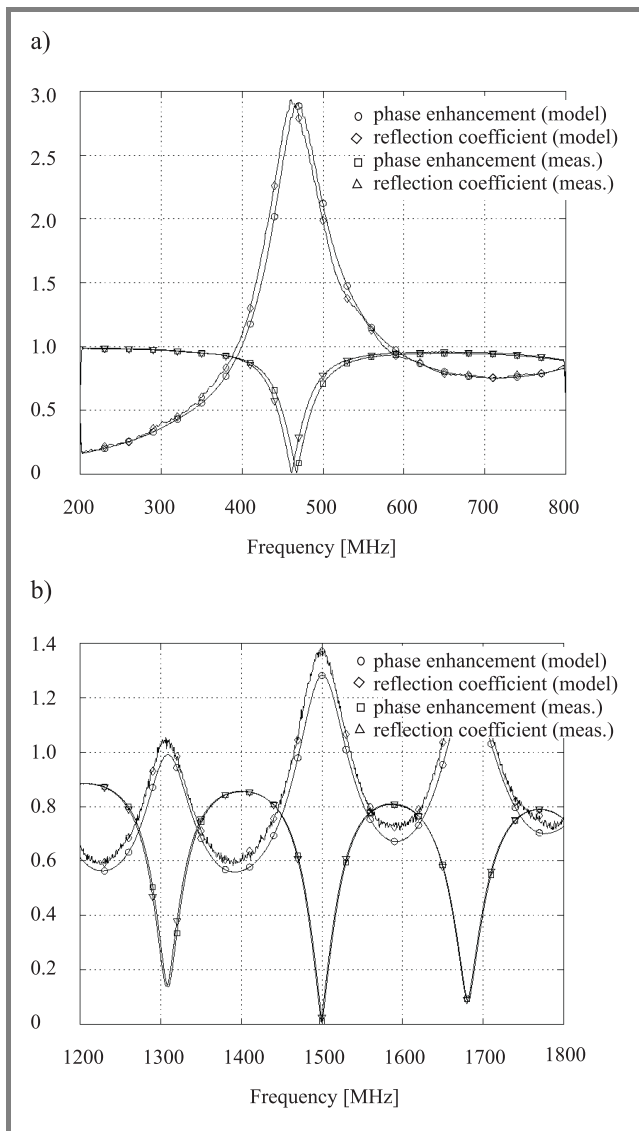


Fig. 6. Modeled and measured link parameters as a function of frequency for design I (a) and design IV (b).

Eq. (13) and the actual measured modulation improvement in Table 1. The slight differences in the predicted resonant frequency (most noticeable in the lowest frequency design) are attributed to extra delay introduced in the measurements when the resonator circuits were separated into components for s -parameter characterization. This error was much less pronounced for the higher frequency designs because the delay offset was a much smaller portion of the overall delay of the cavity. In either case, the delay can be easily characterized and removed.

4. Conclusions

Resonant electrode structures can significantly improve the response of travelling-wave electro-optic modulators over a narrow frequency range, reducing the link loss in radio-on-fiber systems. A simple model of a generic resonant

electrode structure has been developed, and experimental results validate the model and show the potential of resonant electrode structures in improving the performance of radio-on-fiber systems.

It is anticipated that fully integrated resonant electrode designs will outperform the structures shown here since the cavity losses in such modulators would be much lower and the fundamental resonator mode could be utilized at high frequencies. Regardless, all the modulators provided bandwidths requisite of those required for radio-on-fiber systems.

Current work is focusing on designing a resonantly-enhanced modulator structure for millimetre-wave frequencies where the radio-on-fiber system prototype will be deployed. One of the major challenges with operating at these frequencies is that the active region of the modulator must be reduced substantially in order to support the fundamental resonator mode. Novel resonator structures are currently under development to relax this constraint.

Acknowledgements

The authors would like to thank the National Science and Engineering Research Council (NSERC) of Canada, the Alberta Informatics Circle of Research Excellence (iCORE), the University of Calgary, and TRILabs for their financial support of this project.

References

- [1] A. J. Cooper, "Fibre/radio for the provision of cordless/mobile telephony services in access network," *Electron. Lett.*, vol. 26, no. 24, pp. 2054–2056, 1990.
- [2] W. I. Way, "Optical fiber-based microcellular systems: an overview," *IEICE Trans. Commun.*, vol. E76-B, no. 9, pp. 1091–1102, 1993.
- [3] M. Shibutani, T. Kanai, W. Domom, K. Emure, and J. Namiki, "Optical fiber feeder for microcellular mobile communication systems," *IEEE J. Sel. Areas Commun.*, vol. 11, no. 7, pp. 1118–1126, 1993.
- [4] L. Noel, D. Wake, D. G. Moodie, D. D. Marcenac, L. D. Westbrook, and D. Nasset, "Novel techniques for high-capacity 60-GHz fiber-radio transmission systems," *IEEE Trans. Microw. Theory Techn.*, vol. 45, no. 8, pp. 1416–1422, 1997.
- [5] C. H. Cox III, G. E. Betts, and L. M. Johnson, "An analytic and experimental comparison of direct and external modulation in analog fiber-optic links," *IEEE Trans. Microw. Theory Techn.*, vol. 38, no. 5, pp. 501–509, 1990.
- [6] L. A. Molter-Orr, H. A. Haus, and F. J. Leonberger, "20 GHz optical waveguide sampler," *IEEE J. Quant. Electron.*, vol. QE-19, no. 12, pp. 1877–1883, 1983.
- [7] M. Izutsu, H. Murakami, and T. Sueta, "Standing-wave structure optical waveguide modulator using a resonant electrode at 10 GHz," in *Conf. Proc. OFC/IOOC '87*, 1987, p. TUQ32.
- [8] M. Izutsu *et al.*, "Millimeter wave light modulator using LiNbO₃ waveguide with resonant electrode," in *Conf. Proc. CLEO*, 1988, pp. PD14–1.
- [9] G. K. Gopalakrishnan and W. K. Burns, "Performance and modeling of resonantly enhanced LiNbO₃ modulators for low-loss analog fiber-optic links," *IEEE Trans. Microw. Theory Techn.*, vol. 42, no. 12, pp. 2650–2656, 1994.
- [10] Y. S. Visagathilagar, A. Mitchell, and R. B. Waterhouse, "Resonantly enhanced Mach-Zehnder interferometer modulators," in *Conf. Proc. ACOFTAOS'99*, 1999.

- [11] Y. S. Visagathilagar, A. Mitchell, and R. B. Waterhouse, "Fabry-Perot type resonantly enhanced Mach-Zehnder modulator," in *MWP'99 Dig.*, 1999, pp. 17-20.
- [12] D. M. Pozar, *Microwave Engineering*. 2nd ed. Wiley, 1998.



Sean Victor Hum was born in Calgary, Alberta, Canada in 1976. He received his bachelor's degree in 1999 and his master's degree in December 2001, both in electrical engineering from the University of Calgary. Since interning with TRILabs in 1997 he has been involved with various aspects of optical radio systems, with his

master's research focusing on specialized devices for this application. Currently, he is pursuing his doctorate at the U of C in the area of reconfigurable antennas. His research interests lie in the area of reconfigurable RF systems and microwave photonics.

e-mail: svhum@cal.trilabs.ca

TRILabs

University of Calgary

(403) 210-3529 Street NW

Calgary, Alberta, T2L 2K7, Canada



Michał Okoniewski received his MSEE and Ph.D. (with distinction) degrees from the Technical University of Gdańsk, Gdańsk, Poland in 1984 and 1990, respectively. From 1984 to 1986 he was with the Institute of Fluid Flow Machinery, Polish Academy of Sciences, and since 1986 with the Technical University of Gdańsk as

an Assistant Professor. From 1992 to 1994 he was with the University of Victoria, British Columbia, Canada,

as an NSERC International Postdoctoral Fellow and later as a Reserach Fellow and an Adjunct Professor. Since 1998 he has been an Associate Professor at the University of Calgary and a scientist with TRILabs Calgary. In 2002 he was appointed a prestigious CRC Chair position in Applied Electromagnetics. Dr. Okoniewski's current research interests include applied and computational electromagnetics, antennas, passive componets, RF MEMS, microwave photonics, dielectric spectroscopy and confocal microwave microscopy for breast cancer detection. Dr. Okoniewski is a Senior Member of IEEE and an Associate Editor of IEEE Transactions of Antennas and Propagation.

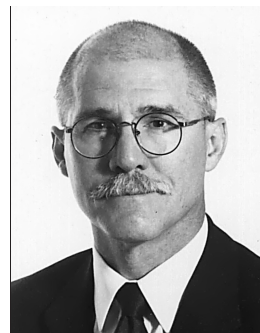
e-mail: michal@enl.ucalgary.ca

Department of Electrical and Computer Engineering

University of Calgary

2500 University Drive NW

Calgary, Alberta, T2N 1N4, Canada



Robert J. Davies received his B.Sc. and M.Sc. degrees in electrical engineering from the University of Calgary, Canada, in 1987 and 1989, respectively. He received his Ph.D. in electrical and computer engineering from the University of Alberta, Canada in 1999. He was a researcher with TELUS Communications in Calgary from 1989

until 1997. He is currently a research scientist with TRILabs in Calgary and an Adjunct Professor at the University of Calgary. His research interests include radio systems, photonics and high speed signal processing. He has 2 patents granted, 4 others pending, and has authored or co-authored 30 papers.

e-mail: davies@cal.trilabs.ca

TRILabs

University of Calgary

280 3553-31 Street NW

Calgary, Alberta, T2L 2K7, Canada